RESEARCH ARTICLE | MARCH 03 2025

Wave interaction with multiple floating elastic plates with arbitrary constraints near a sloping beach

Special Collection: Wave-Structure Interaction

Yifeng Yang ; Luofeng Huang ; Michael H. Meylan

Physics of Fluids 37, 032103 (2025)
https://doi.org/10.1063/5.0257242

Physics of Fluids ARTICLE pubs.aip.org/aip/pof

Wave interaction with multiple floating elastic plates with arbitrary constraints near a sloping beach

Cite as: Phys. Fluids **37**, 032103 (2025); doi: 10.1063/5.0257242
Submitted: 9 January 2025 · Accepted: 4 February 2025 ·
Published Online: 3 March 2025

Yifeng Yang,[1,a)] Luofeng Huang,[2,a)] and Michael H. Meylan[3]

AFFILIATIONS

[1]Department of Mechanical Engineering, University College London, Torrington Place, London, WC1E 7JE, United Kingdom
[2]Faculty of Engineering and Applied Sciences, Cranfield University, Cranfield, MK43 0AL, United Kingdom
[3]School of Information and Physical Sciences, University of Newcastle, Callaghan, NSW 2308, Australia

Note: This paper is part of the Special Topic, Wave-Structure Interaction.
[a)]**Authors to whom correspondence should be addressed:** yifeng.yang.19@ucl.ac.uk and luofeng.huang@cranfield.ac.uk

ABSTRACT

The problem of wave interaction with multiple elastic plates floating near a sloping beach is considered, particularly resembling the case of a floating solar farm near a coast. The linearized shallow water theory is adopted to describe the motion of fluid. The Kirchhoff–Love plate theory is used to model the elastic plates. A highly efficient domain decomposition approach is applied to derive the solution. Particularly, the eigenfunction expansions are employed to establish the velocity potential in free surface fluid domains, while the Green function method is used to construct the velocity potential of the fluid domain covered by floating elastic plates. This approach can significantly reduce the number of unknowns in the velocity potential, especially when a large number of plates are involved. Extensive results and discussions are provided for the wave run-up on the beach, maximum deflection, and principal strain on the elastic plates. In particular, based on a wide space approximated solution, the oscillatory behaviour of the wave run-up vs the incident wavenumber is analysed, along with the corresponding physical mechanisms. Furthermore, apart from the frequency-domain results, time-domain analyses are also conducted based on a Fourier transform approach. Two different types of incident impulses are considered to interact with floating elastic plates near a beach, namely a Gaussian wave packet and a storm-type incident wave.

I. INTRODUCTION

Meeting the world's clean energy goals requires a significant expansion of photovoltaic solar panels, with a focus on deploying floating photovoltaic (FPV) systems in seas in an environment-friendly way.[1] However, due to the uncertainties in the environmental loads in oceans, the designed FPV systems should have strong abilities to resist wave-induced loads and motions.[2] Currently, FPVs are mostly deployed in coastal regions, where they can be applied to generate power for existing marine infrastructures, e.g., harbours and offshore fish farms. However, in coastal regions, water waves can be further reflected by the beach, and produce complex interactions with the floating structures. For the safe operation of FPV systems in seas, it is important to understand the physical mechanism behind such interactions, as well as the potential risks due to wave loads and wave-induced motions on the structures.

For FPVs, solar panels are installed on floaters that can extend for kilometres, creating an expansive floating solar farm (FSF). In this context, the elasticity of the floating structure is crucial and should be considered when investigating its interaction with ocean waves. One approach to model such types of problems involve using the elastic thin plate theory for the floating structures, while the linearized velocity potential is employed for the fluid. The approach has been applied to a series of other types of elastic floating structures, e.g., floating ice sheets in polar and other icy water regions. In particular, Fox and Squire[3] investigated the problem of wave transmission and reflection by a semi-infinite ice sheet based on the method of matched eigenfunction expansion (MEE), where the ice sheet was modelled by the Kirchhoff–Love plate theory, and its edge was assumed to be free to move. The same problem was also considered later by Tkacheva[4] using the Wiener–Hopf technique. Meylan and Squire[5] considered water

wave interaction with a single and double floating ice sheet of finite sizes. In their work, the velocity potential was constructed by employing the Green function and the boundary integral equation. Evans and Porter[6] studied the problem of hydroelastic waves propagating in an infinite ice sheet with a narrow crack, two different procedures one by MEE and another by Green function were proposed in their work. Later, the solution procedure was extended to an finite ice sheet with multiple narrow cracks in Porter and Evans.[7] Williams and Squire[8] solved the problem of wave scattering by three interconnected ice sheets with different physical properties. More recently, Barman, et al.[9] investigated a similar problem to Evans and Porter,[6] while an additional factor that the internal compression stress within the ice sheet was considered. Additional research efforts on wave and ice sheet interactions can be found in the review paper.[10] The literature we discuss is all for the two-dimensional problem, and the extensive literature on the three-dimensional problem can be found in the review paper mentioned above.

In addition to simulating the problems of floating ice sheets, the elastic thin plate model is also applied to study the hydrodynamic performance of Very Large Floating Structures (VLFSs). A key distinction between VLFSs and ice sheets is that VLFSs often involve multiple and various types of physical constraints, e.g., structural hinges, mooring lines, etc. Particularly, Karmakar, et al.[11] studied wave interaction with multiple articulated floating elastic plates covering the entire water surface, based on the method of MEE. Later, Karmakar and Soares[12] investigated the problem of surface wave scattering by a floating elastic plate moored to the seabed. In their work, the mooring lines were located at two side edges of the plate, and modelled as two vertical springs. Singla, et al.[13] studied the hydroelastic responses of an elastic plate in waves, floating near a porous plate. Their work evaluated how the porous plate mitigates the wave-induced structural response on the floating elastic plate. Later, Praveen, et al.[14] investigated water waves interaction with an array of multiple articulated floating elastic plates using the approach of MEE. In their work, the elastic plates were modelled by the Timoshenko–Mindlin thick plate theory to account for the shear deformation and rotational bending effects. Recently, Yang, et al.[15] considered a similar problem and further extended it to treat an arbitrary number and types of physical constraints in floating elastic plates. In the work, instead of using MEE, the velocity potential of the fluid beneath the elastic plates was established by using a boundary integral equation and the Green function for fluid fully covered by an elastic plate.

The studies discussed above focus on the hydroelastic interaction between surface waves and floating elastic plate structures in an unbounded ocean with a flat seabed. However, variable bathymetry is common in real ocean environments, which requires consideration of the effects of an uneven seabed on wave-body interactions. A series of work have been conducted to address this issue. Typically, Wang and Meylan[16] investigated the wave response of a two-dimensional elastic thin plate floating on water of variable depth. In their work, the boundary value problem (BVP) was solved using a hybrid approach, where the entire fluid domain was divided into three subdomains: two semi-infinite fluid regions with constant water depths located before and after the floating plate, and a finite domain containing both the plate and the variable-depth seabed. In two semi-infinite domains, the method of MEE was employed to establish the velocity potential, while in the finite domain, a boundary integral equation was applied to solve the problem numerically. Belibassakis and Athanassoulis[17] considered water wave transmission and reflection by a large body floating in a variable bathymetry region. In their work, the BVP was converted into an equivalent variational equation. Subsequently, a modified MEE method based on that of the constant water-depth problem is proposed to approximate this solution. Later, the procedure was also applied to many other works in variable bathymetry.[18,19] Porter and Newman[20] investigated the problem of regular surface wave diffraction by a vertical circular cylinder standing in an annular region of variable bathymetry, where the mild-slope approximation was used to derive the analytical solution, and it was verified by comparing with that obtained by using the WAMIT solver. Later, Feng, et al.[21] investigated the problem of wave radiation and diffraction by a two-dimensional body floating near a sloping beach. In their work, the boundary element method (BEM) with Ranking sources was applied to derive the solution. Liu *et al.*[22] studied a similar problem as in Belibassakis and Athanassoulis,[17] and employed a hybrid approach, where the floating elastic structures were discretized as a series of modules connected by elastic beams, and then the approach of MEE and BEM were employed to solve the problem numerically. Apart from the scenarios with continuously varying bathymetry, as discussed above, there are also some cases in nature with abrupt changes in water depth. In particular, Kar *et al.*[23] investigated the Bragg resonance due to long waves scattered by an array of floating flexible plates in an ocean environment with multiple submerged trenches. In their work, the linearized shallow water equations, together with the approach of MEE was employed to solve the problem. Similarly, through using the method of MEE, Zhang *et al.*[24] studied the wave resonant response of multiple elastic plates floating in a fluid domain with a sudden change of water depth.

In the present work, we consider a FSF floating near a sloping beach to understand its interaction with water waves in coastal regions. A key feature of the present work is the inclusion of wave reflection effects from the ocean beach, along with the consideration of interactions between water waves and the FSF in a semi-infinite fluid domain. On the one hand, the reflected wave here will affect the hydrodynamic response of the FSF,[20,21] which makes it quite different from that in the unbounded fluid region. On the other hand, the presence of the FSF may also influence the wave conditions in coastal regions, here, by considering the wave run-up on the beach, we illustrate how the deployment of FSF impacts the waves near the shore. To study the problem, the linearized shallow water theory is applied for the fluid, and the solar panel units are modelled as a series of floating elastic plates connected by arbitrary types of physical constraints. The solution here is derived using an efficient domain decomposition method, which is a further extension of the approach in Yang *et al.*[15] to shallow water environment problems. In particular, the eigenfunction expansion is applied to the velocity potential in the free surface regions with flat seabed. In the sloping beach region, the general solution is obtained by applying a variable substitution procedure to the boundary value problem (BVP). By contrast, for the fluid beneath the FSF, an integral equation is used to establish the velocity potential, which makes it highly efficient for modelling floating panels with a large number of arbitrary types of physical constraints. Here, case studies are conducted for two different types of internal constraints, namely the rotational spring hinges and vertical spring conditions. Based on the obtained results, extensive analysis is made on the wave run-up on the beach

and structural responses of the FSF. Particularly the effects of the sloping angle, as well as the properties of the floating elastic plates.

The rest of the paper is arranged as follows. The mathematical modelling of the problem is presented in Sec. II, where the governing equation and boundary conditions of the BVP are presented. In Sec. III, an exact solution procedure based on the decomposition method is introduced, and a wide space approximation is further proposed. The numerical results are discussed in Sec. IV. Finally, the conclusion is given in Sec. V.

II. MATHEMATICAL MODELLING

The problem of long wave interaction with multiple elastic plates connected by arbitrary types of constraints, and float near a sloping beach is sketched in Fig. 1. A Cartesian coordinate system O-xz is defined with the origin located at the intersection of the sloping beach and the still water surface. The positive x-axis is along the mean water surface, and the z-axis points upwards. In the horizontal seabed region, the mean water depth $h(x) = h_0$, and $h(x) = x\tan\beta$ in the sloping beach region, where β denotes the angle of inclination of the beach. A system of elastic plates with internal constraints covering the water surface is located in the horizontal seabed region at $x_2 \le x \le x_3$, with $x_2 \ge x_1 = h_0\cot\beta$. Here, all the elastic plates are assumed to be homogeneous and have identical physical properties. We consider two types of internal constraints, as summarised in Table I. In particular, two adjacent plates are connected by rotational spring hinges at $x = a_i$ $(i = 1 \sim N_a)$ with $x_2 < a_i < a_{i+1} < x_3$, as well as vertical springs are imposed at $x = b_i$ $(i = 1 \sim N_b)$ with $x_2 < b_i < b_{i+1} < x_3$ to model the mooring constraints between the plates and seabed. An incident wave comes from $x = +\infty$ and will be scattered by the elastic plates and reflected by the sloping beach.

The present scenario normally occurs in coastal regions, and the problem is solved under the assumption of the linear long-wave theory in shallow water environment.[25] According to Dean and Dalrymple,[26] the continuity equation can be written as

$$\frac{\partial W(x,t)}{\partial t} + \frac{\partial}{\partial x}\left\{h(x)\frac{\partial \Phi(x,t)}{\partial x}\right\} = 0, \quad 0 < x < +\infty. \tag{1}$$

where $\Phi(x,t)$ and $W(x,t)$ represent the velocity potential and wave elevation respectively. We further assume that the motion of the fluid is sinusoidal in time with frequency ω. Hence, the velocity potential and wave elevation can be written as $\Phi(x,t) = \mathrm{Re}\{\phi(x)e^{\mathrm{i}\omega t}\}$ and $W(x,t) = \mathrm{Re}\{\eta(x)e^{\mathrm{i}\omega t}\}$, where $\phi(x)$ and $\eta(x)$ denote the spatial components of Φ and W respectively, and Eq. (1) becomes

TABLE I. Positions of two different types of internal constraints in the floating elastic plates system.

Edge type	Position
Hinged by rotational springs	$x = a_1, a_2 \ldots a_{N_a}$
Supported by vertical springs	$x = b_1, b_2 \ldots . b_{N_b}$

$$\mathrm{i}\omega\eta(x) + \frac{d}{dx}\left\{h(x)\frac{d\phi(x)}{dx}\right\} = 0, \quad 0 < x < +\infty. \tag{2}$$

The dynamic boundary condition on the free surface is

$$\eta(x) = -\frac{\mathrm{i}\omega}{g}\phi(x), \quad 0 < x < x_2 \quad \& \quad x_3 < x < +\infty. \tag{3}$$

where g denotes the acceleration due to gravity. Substituting Eq. (3) into (2), the governing equation for $\phi(x)$ in the regions with a free surface can be written as

$$\frac{d}{dx}\left\{h(x)\frac{d\phi(x)}{dx}\right\} + \frac{\omega^2}{g}\phi(x) = 0, \quad 0 < x < x_2 \quad \& \quad x_3 < x < +\infty. \tag{4}$$

The boundary condition on the floating elastic plates gives

$$L\frac{d^4\eta(x)}{dx^4} - m_e\omega^2\eta(x) = -\mathrm{i}\omega\phi(x) - \rho g\eta(x), \quad x_2 < x < x_3, \tag{5}$$

where $L = \frac{Eh_e^3}{12(1-\nu^2)}$ and $m_e = \rho_e h_e$ represent the effective flexural rigidity and mass per unit area of the elastic plates. E, ν, ρ_e, and h_e denote the Young's modulus, Poisson's ratio, density and thickness of the plates, respectively. Combining Eqs. (2) and (5) to eliminate $\eta(x)$, and notice $h(x) = h_0$ at $x_2 < x < x_3$, we obtain

$$L\frac{d^6\phi(x)}{dx^6} + \left(\rho g - m_e\omega^2\right)\frac{d^2\phi(x)}{dx^2} + \frac{\rho\omega^2}{h_0}\phi(x) = 0, \quad x_2 < x < x_3. \tag{6}$$

At each physical constraint connecting two adjacent plates, edge conditions should be imposed. From Xia *et al.*,[27] at the rotational spring hinged edge, the deflection, bending moment and the shear force of the plates are continuous, while the jump is on the slope. Notice from Eq. (2), in the region of floating elastic plates, $\eta = \frac{\mathrm{i}h_0}{\omega}\frac{d^2\phi}{dx^2}$, which leads to

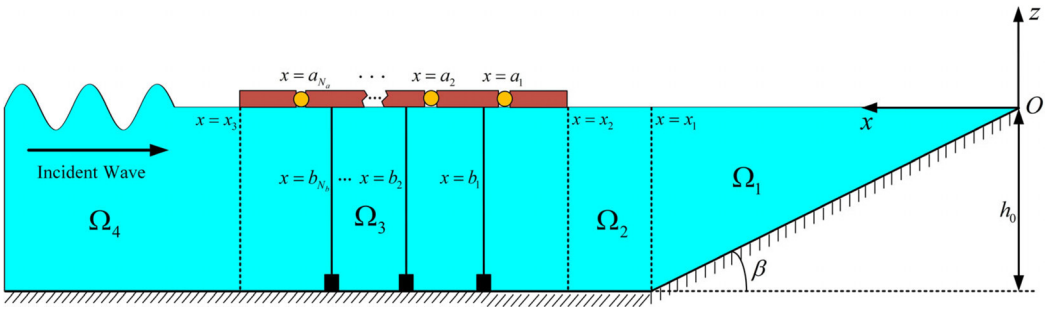

FIG. 1. The sketch of an incoming current interaction with multiple elastic plates connected by arbitrary types of constraints floating near a sloping beach.

$$\begin{cases} \dfrac{d^2\phi(a_i+0^-)}{dx^2} = \dfrac{d^2\phi(a_i+0^+)}{dx^2} \\ L\dfrac{d^4\phi(a_i+0^+)}{dx^4} = L\dfrac{d^4\phi(a_i+0^-)}{dx^4} \\ \quad = \mu^{(i)}\left[\dfrac{d^3\phi(a_i+0^+)}{dx^3} - \dfrac{d^3\phi(a_i+0^-)}{dx^3}\right] \\ \dfrac{d^5\phi(a_i+0^+)}{dx^5} = \dfrac{d^5\phi(a_i+0^-)}{dx^5}, \end{cases} \quad i = 1 \sim N_a, \quad (7a \sim c)$$

where $\mu^{(i)}$ denotes the stiffness of the rotational spring at $x = a_i$. At the position of the vertical spring, the deflection, slope and bending moment of the plate are continuous, and the jump is on the shear force, we have

$$\begin{cases} \dfrac{d^3\phi(b_i+0^-)}{dx^3} = \dfrac{d^3\phi(b_i+0^+)}{dx^3} \\ \dfrac{d^4\phi(b_i+0^-)}{dx^4} = \dfrac{d^4\phi(b_i+0^+)}{dx^4} \\ L\left[\dfrac{d^5\phi(b_i+0^+)}{dx^5} - \dfrac{d^5\phi(b_i+0^-)}{dx^5}\right] \\ \quad = q^{(i)}\dfrac{d^2\phi(b_i+0^+)}{dx^2} = q^{(i)}\dfrac{d^2\phi(b_i+0^-)}{dx^2}, \end{cases} \quad i = 1 \sim N_b, \quad (8a \sim c)$$

where $q^{(i)}$ represents the stiffness of the vertical spring at $x = b_i$.

At two side edges of the entire elastic plates system, the edge conditions are[12]

$$\frac{d^4\phi(x_2)}{dx^4} = 0, \quad \frac{d^4\phi(x_2)}{dx^4} = 0 \quad (9a)$$

$$L\frac{d^5\phi(x_2)}{dx^5} = q^r\frac{d^2\phi(x_2)}{dx^2}, \quad L\frac{d^5\phi(x_3)}{dx^5} = q^l\frac{d^2\phi(x_3)}{dx^2} \quad (9b)$$

where q^r and q^l represent the stiffness of vertical springs at $x = x_2$ and x_3 respectively. If $q^r = q^l = 0$, Eqs. (9a) and (9b) means zero shear force and bending moment, which correspond to the free edge conditions. If q^r and q^l are non-zero, Eq. (9b) is used to model the plate system connecting to the seabed by two mooring lines with stiffness q^r and q^l respectively. Furthermore, apart from all the conditions listed above, the far-field boundary condition should be imposed at $x = +\infty$ to ensure waves propagating outwards.

III. SOLUTION PROCEDURE

A. Solution procedure based on the domain decomposition approach

The domain decomposition approach is employed to solve the boundary value problem. To do that, the entire fluid domain is divided into 4 subdomains. Namely, Ω_1 $(0 < x < x_1)$, Ω_2 $(x_1 < x < x_2)$, Ω_3 $(x_2 < x < x_3)$, and Ω_4 $(x_3 < x < +\infty)$, as illustrated in Fig. 1. In each subdomain Ω_i, the spatial velocity potential and wave elevation are denoted by $\phi^{(i)}$ and $\eta^{(i)}$ $(i = 1\text{–}4)$ respectively. $\phi^{(1)}$, $\phi^{(2)}$, and $\phi^{(4)}$ can be constructed by solving the corresponding ordinary different equation (ODE) directly. By contrast, $\phi^{(3)}$ is constructed through an integral equation. These velocity potentials are matched at their interfaces to obtain the final solution.

Following the discussion above, in Ω_2 and Ω_4, the mean water depth $h(x) = h_0$ is a constant. Hence, Eq. (4) becomes

$$\frac{d^2\phi^{(i)}(x)}{dx^2} + \frac{\omega^2}{gh_0}\phi^{(i)}(x) = 0, \quad i = 2, 4. \quad (10)$$

From Eq. (10), $\phi^{(2)}(x)$ and $\phi^4(x)$ can be solved as

$$\phi^{(2)}(x) = I^{(2)}e^{ik_0x} + R^{(2)}e^{-ik_0x}, \quad (11)$$

$$\phi^{(4)}(x) = Ie^{ik_0x} + R^{(4)}e^{-ik_0x}, \quad (12)$$

where $k_0 = \omega/\sqrt{gh_0}$ represents the wave number, $I = iAg/\omega$ and A represents the amplitude of the incident wave, $I^{(2)}$, $R^{(2)}$, and $R^{(4)}$ are unknown coefficients.

In Ω_1, applying $h(x) = h_0\tan\beta$ to Eq. (4), we have

$$\frac{x\tan\beta}{h_0}\frac{d^2\phi^{(1)}(x)}{dx^2} + \frac{\tan\beta}{h_0}\frac{d\phi^{(1)}(x)}{dx} + k_0^2\phi^{(1)}(x) = 0. \quad (13)$$

To solve Eq. (13), we may apply a variable substitution procedure,[28] let $\xi = 2k_0\sqrt{xh_0\cot\beta}$, we obtain

$$\frac{d^2\phi^{(1)}}{d\xi^2} + \frac{1}{\xi}\frac{d\phi^{(1)}}{d\xi} + \phi^{(1)} = 0. \quad (14)$$

Equation (14) is the zero-th order Bessel equation. Since $\phi^{(1)}$ should be finite at $x = 0$, we obtain

$$\phi^{(1)}(x) = A^{(1)}\mathcal{J}_0(\xi) = A^{(1)}\mathcal{J}_0\left(2k_0\sqrt{xh_0\cot\beta}\right), \quad (15)$$

where $A^{(1)}$ denotes an unknown coefficient, $\mathcal{J}_n$ represents the n-th order Bessel function of the first kind.

To solve the $\phi^{(3)}$, we first consider a Green function G, which corresponds to a fluid domain of an infinite extent fully covered by a perfect and homogeneous elastic plate. From Eq. (5), the governing equation of G can be written as

$$L\frac{\partial^6 G}{\partial x^6} + (\rho g - m_e\omega^2)\frac{\partial^2 G}{\partial x^2} + \frac{\rho\omega^2}{h_0}G = \delta(x-\zeta), \quad -\infty < x < +\infty, \quad (16)$$

where δ denotes the Dirac delta function, and ζ is the source position. G can be solved through a Fourier transform procedure, which provides

$$G(x,\zeta) = -\frac{1}{2\pi}\int_{-\infty}^{+\infty}\frac{e^{i\alpha(x-\zeta)}}{L\alpha^6 + (\rho g - m_e\omega^2)\alpha^2 - \frac{\rho\omega^2}{h_0}}d\alpha, \quad (17)$$

where the integration path in Eq. (17) should pass over (under) the pole at $\alpha = +\kappa_0$ $(-\kappa_0)$ to ensure waves propagate outwards. κ_0 is the unique positive real root of the equation $L\alpha^6 + (\rho g - m_e\omega^2)\alpha^2 - \frac{\rho\omega^2}{h_0} = 0$. Applying the theorem of residue to Eq. (17), $G(x,\zeta)$ can be converted to a series form as

$$G(x,\zeta) = i\sum_{m=-2}^{0}\frac{e^{-i\kappa_m|x-\zeta|}}{6L\kappa_m^5 + 2(\rho g - m_e\omega^2)\kappa_m}, \quad (18)$$

where κ_{-1} and κ_{-2} are two fully complex roots of $L\alpha^4 - (\rho g - m_e\omega^2)\alpha^2 + \frac{\rho\omega^2}{h_0} = 0$ with negative imaginary parts, as well as

satisfying $\bar{\kappa}_{-1} = -\kappa_{-2}$. It is noted that Eq. (18) can be also obtained by applying the shallow water limit to the Green function of finite water depth derived in Evans and Porter.[6]

To obtain $\phi^{(3)}$, we may first write it as

$$\phi^{(3)}(x) = \sum_{m=-2}^{0} \left(C_m e^{i\kappa_m x} + D_m e^{-i\kappa_m x}\right) + \hat{\phi}^{(3)}(x), \tag{19}$$

where C_m and D_m are unknown coefficients. The summation term in Eq. (20) is a general eigenfunction expansion, which is used to satisfy the edge conditions and continuous conditions at $x = x_2$ and x_3. $\hat{\phi}^{(3)}(x)$ is for the conditions at internal constraints, which can be constructed through the following integral equation,

$$\hat{\phi}^{(3)}(x) = \int_{x_2}^{x_3} \left\{ \begin{array}{l} \hat{\phi}^{(3)}(\zeta)\left[L\dfrac{\partial^6 G}{\partial \zeta^6} + (\rho g - m_e\omega^2)\dfrac{\partial^2 G}{\partial \zeta^2}\right] \\ -G\left[L\dfrac{d^6\hat{\phi}^{(3)}(\zeta)}{d\zeta^6} + (\rho g - m_e\omega^2)\dfrac{d^2\hat{\phi}^{(3)}(\zeta)}{d\zeta^2}\right] \end{array} \right\} d\zeta. \tag{20}$$

Applying integration by parts to Eq. (20), which provides

$$\begin{aligned} \hat{\phi}^{(3)}(x) = {} & L\sum_{i=1}^{N_a}\left[\left(\hat{\phi}^{(3)}\frac{\partial^5 G}{\partial\zeta^5} - G\frac{d^5\hat{\phi}^{(3)}}{d\zeta^5}\right) - \left(\frac{d\hat{\phi}^{(3)}}{d\zeta}\frac{\partial^4 G}{\partial\zeta^4} - \frac{\partial G}{\partial\zeta}\frac{d^4\hat{\phi}^{(3)}}{d\zeta^4}\right)\right. \\ & \left. + \left(\frac{d^2\hat{\phi}^{(3)}}{d^2\zeta}\frac{\partial^3 G}{\partial\zeta^3} - \frac{\partial^2 G}{\partial\zeta^2}\frac{d^3\hat{\phi}^{(3)}(x)}{d\zeta^3}\right)\right]_{x=a_i+0^-}^{x=a_i+0^+} \\ & + L\sum_{i=1}^{N_b}\left[\left(\hat{\phi}^{(3)}\frac{\partial^5 G}{\partial\zeta^5} - G\frac{d^5\hat{\phi}^{(3)}(x)}{d\zeta^5}\right)\right. \\ & - \left(\frac{d\hat{\phi}^{(3)}}{d\zeta}\frac{\partial^4 G}{\partial\zeta^4} - \frac{\partial G}{\partial\zeta}\frac{d^4\hat{\phi}^{(3)}}{d\zeta^4}\right) \\ & \left. + \left(\frac{d^2\hat{\phi}^{(3)}}{d^2\zeta}\frac{\partial^3 G}{\partial\zeta^3} - \frac{\partial^2 G}{\partial\zeta^2}\frac{d^3\hat{\phi}^{(3)}}{d\zeta^3}\right)\right]_{x=b_i+0^+}^{x=b_i+0^-}. \end{aligned} \tag{21}$$

Notice $\hat{\phi}^{(3)}$ and $\partial\hat{\phi}^{(3)}/\partial x$ are continuous at $x = a_j$ $(j = 1 \sim N_a)$ and b_j $(j = 1 \sim N_b)$ due to the continuous of velocity potential and pressure, Besides, invoking the edge conditions in Eqs. (7) and (8), we obtain

$$\begin{aligned} \hat{\phi}^{(3)}(x) = {} & \sum_{i=1}^{N_a}\left(\frac{\partial^2 G}{\partial\zeta^2}\frac{d^3\hat{\phi}^{(3)}(x)}{d\zeta^3}\right)_{x=a_i+0^-}^{x=a_i+0^+} \\ & + \sum_{i=1}^{N_b}\left(G\frac{d^5\hat{\phi}^{(3)}(x)}{d\zeta^5}\right)_{x=b_i+0^-}^{x=b_i+0^+}. \end{aligned} \tag{22}$$

Define

$$E_i = \left(\frac{d^3\hat{\phi}^{(3)}(x)}{d\zeta^3}\right)_{x=a_i+0^-}^{x=a_i+0^+} \tag{23a}$$

$$F_i = \left(\frac{d^5\hat{\phi}^{(3)}(x)}{d\zeta^5}\right)_{x=b_i+0^-}^{x=b_i+0^+} \tag{23b}$$

as physical parameters jump at edges at $x = a_i$ and b_i. Substituting Eqs. (22) and (23) into Eq. (19), we obtain

$$\begin{aligned} \phi^{(3)}(x) = {} & \sum_{m=-2}^{0}\left(C_m e^{i\kappa_m x} + D_m e^{-i\kappa_m x}\right) + \sum_{i=1}^{N_a} E_i\frac{\partial^2 G(x,a_i)}{\partial\zeta^2} \\ & + \sum_{i=1}^{N_b} F_i G(x,b_i). \end{aligned} \tag{24}$$

Using the Green function and the integral equation to construct $\phi^{(3)}(x)$ can significantly reduce the number of unknowns, particularly when dealing with a large number of plates. Typically, in Eq. (24), there is a total of $N_a + N_b + 6$ unknowns, namely C_m & D_m $(m = -2 \sim 0)$, E_i $(i = 1 \sim N_a)$ and F_i $(i = 1 \sim N_b)$. By contrast, if we expand the velocity potentials of the fluid below each single plate as an eigenfunction series, and match them at the interface. There will be six unknowns in each velocity potential, and a total of $6(N_a + N_b + 1)$ unknowns. In such a case, it can be found then the total number of unknowns is significantly reduced by using the present method.

To solve all the unknowns in $\phi^{(j)}$ $(j = 1$–$4)$, we may use the continuous conditions at the interfaces for the velocity potential and dynamic pressure at $x = x_j$ $(i = 1, 2, 3)$, or

$$\phi^{(1)}(x_1) = \phi^{(2)}(x_1), \quad \frac{\partial\phi^{(1)}(x_1)}{\partial x} = \frac{\partial\phi^{(2)}(x_1)}{\partial x} \tag{25a}$$

$$\phi^{(2)}(x_2) = \phi^{(3)}(x_2), \quad \frac{\partial\phi^{(2)}(x_2)}{\partial x} = \frac{\partial\phi^{(3)}(x_2)}{\partial x} \tag{25b}$$

$$\phi^{(3)}(x_3) = \phi^{(4)}(x_3), \quad \frac{\partial\phi^{(3)}(x_3)}{\partial x} = \frac{\partial\phi^{(4)}(x_3)}{\partial x}. \tag{25c}$$

Equation (25a) provides

$$\mathcal{J}_0(2k_0x_1)A^{(1)} - e^{ik_0x_1}I^{(2)} - e^{-ik_0x_1}R^{(2)} = 0 \tag{26a}$$

$$k_0\mathcal{J}_1(2k_0x_1)A^{(1)} + ik_0e^{ik_0x_1}I^{(2)} - ik_0e^{-ik_0x_1}R^{(2)} = 0. \tag{26b}$$

Equation (25b) gives

$$e^{ik_0x_2}I^{(2)} + e^{-ik_0x_2}R^{(2)} - \left\{ \begin{array}{l} \displaystyle\sum_{m=-2}^{0}\left(e^{i\kappa_m x_2}C_m + e^{-i\kappa_m x_2}D_m\right) \\ \displaystyle+\sum_{i=1}^{N_a}\frac{\partial^2 G(x_2,a_i)}{\partial\zeta^2}E_i + \sum_{i=1}^{N_b}G(x_2,b_i)F_i \end{array} \right\} = 0 \tag{27a}$$

$$\begin{aligned} & ik_0e^{ik_0x_2}I^{(2)} - ik_0e^{-ik_0x_2}R^{(2)} \\ & - \left\{ \begin{array}{l} \displaystyle i\sum_{m=-2}^{0}\kappa_m\left(e^{i\kappa_m x_2}C_m - e^{-i\kappa_m x_2}D_m\right) \\ \displaystyle+\sum_{i=1}^{N_a}\frac{\partial^3 G(x_2,a_i)}{\partial x\partial\zeta^2}E_i + \sum_{i=1}^{N_b}\frac{\partial G(x_2,b_i)}{\partial x}F_i \end{array} \right\} = 0. \end{aligned} \tag{27b}$$

Equation (25c) gives

$$\left\{\begin{array}{l}\sum_{m=-2}^{0}\left(e^{\mathrm{i}\kappa_m x_3}C_m+e^{-\mathrm{i}\kappa_m x_3}D_m\right)\\ +\sum_{i=1}^{N_a}\frac{\partial^2 G(x_3,a_i)}{\partial\zeta^2}E_i+\sum_{i=1}^{N_b}G(x_3,b_i)F_i\end{array}\right\}-e^{-\mathrm{i}k_0x_3}R^{(4)}=Ie^{\mathrm{i}k_0x_3} \tag{28a}$$

$$\left\{\begin{array}{l}\mathrm{i}\sum_{m=-2}^{0}\kappa_m\left(e^{\mathrm{i}\kappa_m x_3}C_m-e^{-\mathrm{i}\kappa_m x_3}D_m\right)\\ +\sum_{i=1}^{N_a}\frac{\partial^3 G(x_3,a_i)}{\partial x\partial\zeta^2}E_i+\sum_{i=1}^{N_b}\frac{\partial G(x_3,b_i)}{\partial x}F_i\end{array}\right\}+\mathrm{i}k_0e^{-\mathrm{i}k_0x_3}R^{(4)}=\mathrm{i}k_0Ie^{\mathrm{i}k_0x_3}. \tag{28b}$$

In addition to the equations established in Eqs. (26)–(28). The remaining equations can be obtained from the edge conditions at all the physical constraints. In particular, at $x=a_j$ ($j=1\sim N_a$), substituting Eq. (24) into Eq. (7b), we have

$$\begin{aligned}&L\sum\nolimits_{m=-2}^{0}\kappa_m^4\left(e^{\mathrm{i}\kappa_m a_j}C_m+e^{-\mathrm{i}\kappa_m a_j}D_m\right)+\sum\nolimits_{i=1}^{N_a}\left\{L\frac{\partial^6 G(a_j,a_i)}{\partial x^4\partial\zeta^2}-\mu^{(j)}\left[\frac{\partial^5 G(a_j+0^+,a_i)}{\partial x^3\partial\zeta^2}-\frac{\partial^5 G(a_j+0^-,a_i)}{\partial x^3\partial\zeta^2}\right]\right\}E_i\\&+\sum\nolimits_{i=1}^{N_b}\left\{L\frac{\partial^4 G(a_j,b_i)}{\partial x^4}-\mu^{(j)}\left[\frac{\partial^3 G(a_j+0^+,b_i)}{\partial x^3}-\frac{\partial^3 G(a_j+0^-,b_i)}{\partial x^3}\right]\right\}F_i=0,\quad j=1\sim N_a.\end{aligned} \tag{29}$$

At $x=b_j$ ($j=1\sim N_b$), from Eq. (8c), we have

$$\begin{aligned}&q^{(j)}\sum\nolimits_{m=-2}^{0}\kappa_m^2\left(e^{\mathrm{i}\kappa_m b_j}C_m+e^{-\mathrm{i}\kappa_m b_j}D_m\right)+\sum\nolimits_{i=1}^{N_a}\left\{L\left[\frac{\partial^7 G(b_j+0^+,a_i)}{\partial x^5\partial\zeta^2}-\frac{\partial^7 G(b_j+0^-,a_i)}{\partial x^5\partial\zeta^2}\right]-q^{(j)}\frac{\partial^4 G(b_j,a_i)}{\partial x^2\partial\zeta^2}\right\}E_i\\&+\sum\nolimits_{i=1}^{N_b}\left\{L\left[\frac{\partial^5 G(b_j+0^+,b_i)}{\partial x^5}-\frac{\partial^5 G(b_j+0^-,b_i)}{\partial x^5}\right]-q^{(j)}\frac{\partial^2 G(b_j,b_i)}{\partial x^2}\right\}F_i,\\&j=1\tilde{}N_b.\end{aligned} \tag{30}$$

At $x=x_2$ and x_3, Eqs. (9a) and (9b) provides

$$\sum\nolimits_{m=-2}^{0}\kappa_m^4\left(e^{\mathrm{i}\kappa_m x_j}C_m+e^{-\mathrm{i}\kappa_m x_j}D_m\right)+\sum\nolimits_{i=1}^{N_a}\frac{\partial^6 G(x_j,a_i)}{\partial x^4\partial\zeta^2}E_i+\sum\nolimits_{i=1}^{N_b}\frac{\partial^4 G(x_j,b_i)}{\partial x^4}F_i=0,\quad j=2,\,3. \tag{31}$$

$$\begin{aligned}&\sum_{m=-2}^{0}\kappa_m^2\left[\left(\mathrm{i}L\kappa_m^3+q^r\right)e^{\mathrm{i}\kappa_m x_2}C_m-\left(\mathrm{i}L\kappa_m^3-q^r\right)e^{-\mathrm{i}\kappa_m x_2}D_m\right]+\sum_{i=1}^{N_a}\left[L\frac{\partial^7 G(x_2,a_i)}{\partial x^5\partial\zeta^2}-q^r\frac{\partial^4 G(x_2,a_i)}{\partial x^2\partial\zeta^2}\right]E_i\\&+\sum_{i=1}^{N_b}\left[L\frac{\partial^5 G(x_2,b_i)}{\partial x^5}-q^r\frac{\partial^2 G(x_2,b_i)}{\partial x^2}\right]F_i=0,\end{aligned} \tag{32a}$$

$$\begin{aligned}&\sum_{m=-2}^{0}\kappa_m^2\left[\left(\mathrm{i}L\kappa_m^3+q^l\right)e^{\mathrm{i}\kappa_m x_3}C_m-\left(\mathrm{i}L\kappa_m^3-q^l\right)e^{-\mathrm{i}\kappa_m x_3}D_m\right]+\sum_{i=1}^{N_a}\left[L\frac{\partial^7 G(x_3,a_i)}{\partial x^5\partial\zeta^2}-q^l\frac{\partial^4 G(x_3,a_i)}{\partial x^2\partial\zeta^2}\right]E_i\\&+\sum_{i=1}^{N_b}\left[L\frac{\partial^5 G(x_3,b_i)}{\partial x^5}-q^l\frac{\partial^2 G(x_3,b_i)}{\partial x^2}\right]F_i=0.\end{aligned} \tag{32b}$$

There is a total of N_a+N_b+10 unknows ($A^{(1)}$, $I^{(2)}$, $R^{(2)}$, $C_{-2}\sim C_0$, $D_{-2}\sim D_0$, $R^{(4)}$, $E_1\sim E_{N_a}$, $F_1\sim F_{N_b}$). Eqs. (26)–(28) provides 6 equations, Eqs. (29)–(32) provide N_a+N_b+4 equations. Hence, the total number of equations is consistent to the total number of unknowns, and a unique solution can be obtained.

B. Wide space approximation of the solution

When the floating plate is located far away from the sloping beach, or $x_2\gg x_1$. The solution shown in Sec. III A can be simplified based on the wide space approximation. To do that, we may define the velocity potentials ψ_L and ψ_R for the case of the elastic plates system floating in an unbounded ocean, where the subscript L and R denote the incoming wave from $x=+\infty$ and $x=-\infty$ respectively. Here, we may assume that the right-side edge of the plates system is located at the origin, or $x_2=0$. Hence, we may write

$$\psi_L(x) = \begin{cases} e^{ik_0x} + R_L e^{-ik_0x} & x > x_3 \\ T_L e^{ik_0x} & x < x_2, \end{cases} \tag{33}$$

$$\psi_R(x) = \begin{cases} e^{-ik_0x} + R_R e^{ik_0x} & x < x_2 \\ T_R e^{-ik_0x} & x > x_3, \end{cases} \tag{34}$$

where R_L & T_L and R_R & T_R correspond to the reflection & transmission coefficients of $\psi_L(x)$ and $\psi_R(x)$ respectively. If the plates system is symmetric about its centre, we have $T_L = T_R$ and $R_L = R_R$. We may further introduce the velocity potential $\psi_0(x)$ for the case only with a sloping beach (the case without plates shown in Fig. 1), From Eqs. (11) and (15), $\psi_0(x)$ may be written as

$$\psi_0(x) = \begin{cases} t_s \mathcal{J}_0\left(2k_0\sqrt{xh_0\cot\beta}\right) & 0 < x < h_0\cot\beta \\ e^{ik_0x} + r_s e^{-ik_0x} & x > h_0\cot\beta, \end{cases} \tag{35}$$

where

$$t_s = \frac{2e^{ik_0h_0\cot\beta}}{\mathcal{J}_0(2k_0h_0\cot\beta) + i\mathcal{J}_1(2k_0h_0\cot\beta)} \tag{36a}$$

$$r_s = \frac{\mathcal{J}_0(2k_0h_0\cot\beta) - i\mathcal{J}_1(2k_0h_0\cot\beta)}{\mathcal{J}_0(2k_0h_0\cot\beta) + i\mathcal{J}_1(2k_0h_0\cot\beta)} e^{i2k_0h_0\cot\beta}. \tag{36b}$$

The velocity potential near the plates system can be written as

$$\phi(x) = \psi_L(x - x_2) + \xi\psi_R(x - x_2), \tag{37}$$

where ξ is an unknown coefficient. The velocity potential near the sloping beach ($x < x_2$) can be written as

$$\phi(x) = \epsilon\psi_0(x). \tag{38}$$

where ϵ is an unknown coefficient. Hence, the consistency of the velocity potential in the domain $x_1 < x < x_2$ requires

$$\epsilon = \frac{T_L e^{ik_0x_2}}{e^{i2k_0x_2} - r_sR_R} \tag{39a}$$

$$\xi = \frac{r_sT_L}{e^{i2k_0x_2} - r_sR_R}. \tag{39b}$$

Equations (39a) and (39b) indicate that the solution may show fluctuation trends with several physical parameters, namely the transmission T_L and reflection coefficients R_R of the plate systems, as well as the position of the plates x_2.

IV. NUMERICAL RESULTS AND DISCUSSION

The physical parameters used in Karmakar, et al.[11] are selected in the following computation. In particular, the mean water depth $h_0 = 10$ m, the water density $\rho = 1025\,\mathrm{kg\,m^{-3}}$, and the acceleration due to gravity $g = 9.8\,\mathrm{m\,s^{-2}}$. Besides, all the numerical results are presented in nondimensionalized forms based on a combination of ρ, g, and h_e. In particular, the following parameters are used in the properties of the plates

$$\begin{cases} h_0/h_e = 10 & \rho_e/\rho = 0.9 \\ E/\rho g h_e = 4.9776 \times 10^5 & \nu = 0.3. \end{cases} \tag{40}$$

Besides, $\tilde{\mu}^{(i)} = \mu^{(i)}/\rho g h_e^4$, $\tilde{q}^{(i)} = q^{(i)}/\rho g h_e^2$, $\tilde{q}^r = q^r/\rho g h_e^2$, and $\tilde{q}^l = q^l/\rho g h_e^2$ are defined as nondimensionalized spring stiffness. Moreover, under the shallow water approximation, the wave number range $0 < k_0h_0 < 1$ is considered. The wave run-up A_b on the beach is approximated by the wave elevation at $x = 0$,[28,29] or

$$A_b \approx |\eta(0)| = \frac{\omega}{g}|\phi^{(1)}(0)| = \frac{\omega}{g}|A^{(1)}|. \tag{41}$$

Under the wide space approximation and using Eqs. (35) and (39), A_b can be further approximated as

$$A_b \approx \frac{\omega}{g}\frac{|T_Lt_s|}{|e^{i2k_0x_2} - r_sR_R|}. \tag{42}$$

A. Wave interaction with a single elastic plate near a sloping beach

The case of a single elastic plate floating near a sloping beach is first considered. The results of wave run-up on the beach A_b/A vs k_0h_0 under different plate lengths d (here, $d = x_3 - x_2$) and edge conditions are shown in Fig. 2, where $x_2 - x_1 = h_0$ and the angle of the beach $\beta = 45^\circ$ are fixed. In Fig. 2(a), two side edges of the plate are free to move. It can be observed that when d/h_0 is small, the floating elastic plate only has little effect on A_b/A. The curve of A_b/A vs k_0h_0 at $d/h_0 = 1$ closely resembles that of the case without any plate.[28]

As d/h_0 increases, it becomes evident that A_b/A gradually exhibits oscillations with k_0h_0. It is known from Eq. (42) that such oscillation is in fact related to the oscillatory nature of T_L (R_L), which corresponds to the transmission (reflection) coefficient for the single elastic plate floating in an unbounded ocean, as defined in Sec. III B. As discussed by Meylan and Squire,[30] R_L oscillates with k_0d. The larger value of d, the more pronounced the oscillations in R_L. As shown in Fig. 3(a), $|R_L|$ shows a similar fluctuation trend with A_b/A. In Figs. 2(b)–2(d), apart from using the free edges conditions at $x = x_2$ and x_3. The vertical spring conditions with $\tilde{q}_r = \tilde{q}_l$ are applied. It is found that the variation of A_b/A vs k_0h_0 is extensively changed when vertical springs are used, even when d/h_0 is small. Besides, in Fig. 2(d), when $\tilde{q}_r = \tilde{q}_l \to +\infty$, or under pinned conditions, significantly larger oscillations are observed compared to the free-edge case. This is because larger stiffness values for $\tilde{q}_r$ and $\tilde{q}_l$ result in more pronounced fluctuations in T_L (R_L),[12] and is shown in Fig. 3(b), such behaviour is further reflected in A_b/A.

The scenario of a single elastic plate floating at different transverse locations is considered next. The results of the wave run-up A_b/A vs k_0h_0 are shown in Fig. 4, where the angle $\beta = 45^\circ$ and free edge conditions are applied to the edges of the plate. From Figs. 4(a)–4(d), it is observed that the curves of A_b/A vs k_0h_0 exhibit more fluctuations as k_0h_0 increases. This behaviour results from the oscillatory term $e^{2ik_0x_2}$ in the denominator of Eq. (42). Furthermore, when the distance between the plate and the beach is small, as shown in Fig. 4(a) for $x_2 - x_1 = 10h_0$, significant differences can be observed in A_b/A computed using Eq. (41) and the wide-space approximations obtained from Eq. (42), particularly in the range $0.3 < k_0h_0 < 0.9$. As k_0h_0 increases, this difference gradually diminishes, and the two results become increasingly consistent.

The results of the wave run-up A_b/A on sloping beaches with different angles are shown in Fig. 5, where a single plate of length $d = 10h_0$ floats at $x_2 = x_1 + 50h_0$. In all cases, it is observed that A_b/A oscillates with the variation of k_0h_0, following the trend of the cases without the plate. From Figs. 5(a)–5(d), it is observed that the fluctuation amplitude decreases with a larger sloping angle β. Additionally, for a fixed value of β, the oscillation amplitude of A_b/A in the case of a free-edge plate is much smaller than that for a

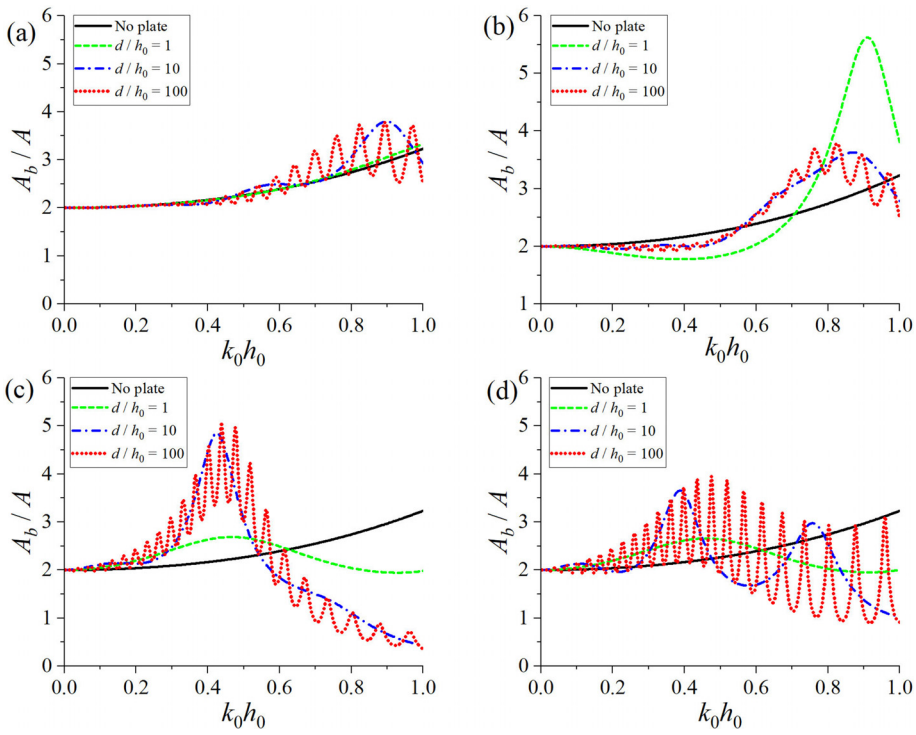

FIG. 2. Wave run-up on the beach vs k_0h_0 under different plate length d and vertical spring stiffness $\tilde{q}^r$ and $\tilde{q}^l$. (a) $\tilde{q}^r = \tilde{q}^l = 0$ (Free); (b) $\tilde{q}^r = \tilde{q}^l = 2$; (c) $\tilde{q}^r = \tilde{q}^l = 20$; and (d) $\tilde{q}^r = \tilde{q}^l = +\infty$ (Pinned). ($\beta = 45^o$, $(x_2 - x_1)/h_0 = 1$, $N_a = N_b = 0$)

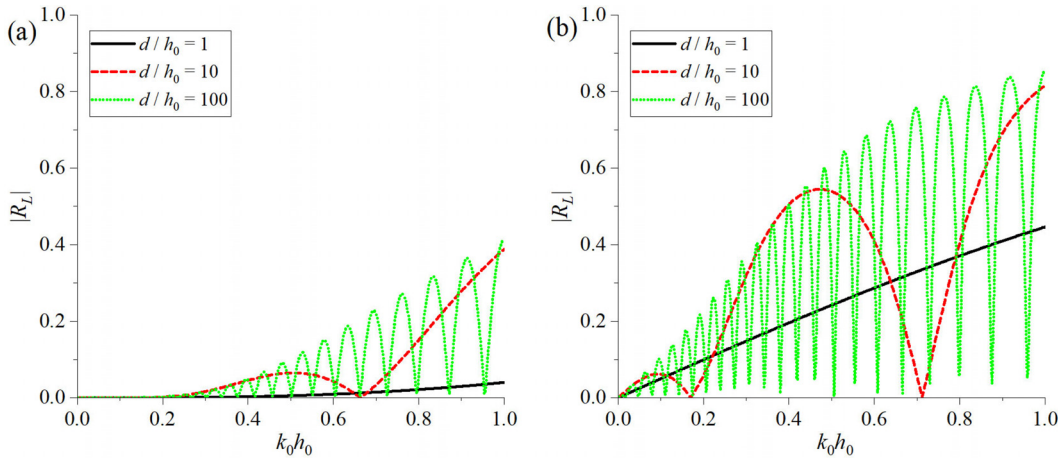

FIG. 3. The reflection coefficient $|R_L|$ vs k_0h_0 for a single floating elastic plate in an unbounded ocean. (a) $\tilde{q}^r = \tilde{q}^l = 0$ (Free); (b) $\tilde{q}^r = \tilde{q}^l = +\infty$ (Pinned).

pinned-edge plate, which is consistent with the phenomenon observed in Fig. 2. Furthermore, with the introduction of the floating plate, it is interesting to see that A_b/A is significantly reduced at certain frequencies. This suggests that the deployment of a floating solar farm could potentially reduce wave run-up on the beaches.

B. Wave interaction with multiple elastic plates near a sloping beach

The scenarios involving multiple elastic plates floating near a sloping beach are further considered. It is assumed that the length of each plate is $d = h_0$, and for an $(N_a + 1)$-plate system, the position of each spring hinged point is

$$a_i = x_2 + id, \quad i = 1 \sim N_a. \tag{43}$$

It is also assumed that the stiffness of each rotational hinge is the same, or $\tilde{\mu}^{(i)} = \tilde{\mu}$. The results of A_b/A vs k_0h_0 under $N_a = 9$ and $N_a = 99$ are shown in Fig. 6, where three different values of $\tilde{\mu}$ are considered. When $\tilde{\mu} = 0$, the bending moment at each hinged point is zero. As shown in Figs. 6(a) and 6(b), the oscillatory behaviour of A_b/A vs k_0h_0

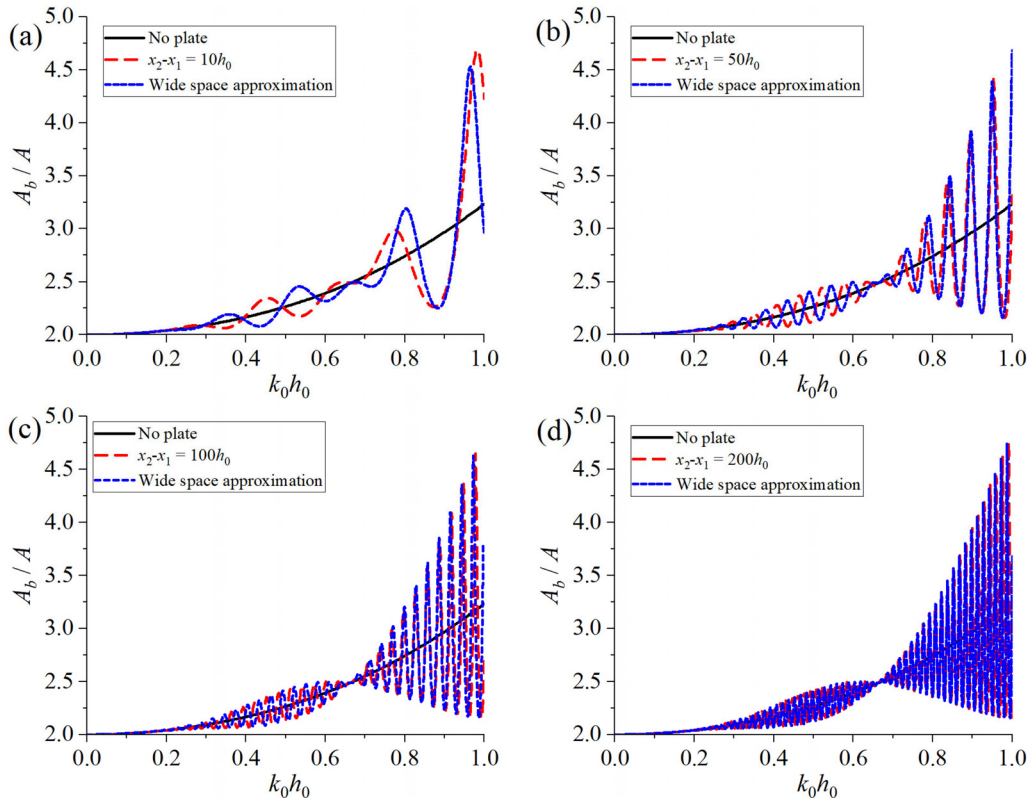

FIG. 4. Wave run-up on the beach vs k_0h_0 when the floating elastic plate is at different positions. (a) $(x_2 - x_1)/h_0 = 10$; (b) $(x_2 - x_1)/h_0 = 50$; (c) $(x_2 - x_1)/h_0 = 100$; and (d) $(x_2 - x_1)/h_0 = 200$. ($\beta = 45^0$, $d/h_0 = 10$, $N_a = N_b = 0$, free at $x = x_2$ & x_3)

is relatively weak in both cases. As $\tilde{\mu}$ increases, the oscillatory behaviours of A_b/A gradually become more pronounced. When $\tilde{\mu}$ is sufficiently large, from Eq. (7b), the rotational spring edge condition approaches the slope continuity condition, causing the multiple-plate system to behave like a single plate. In particular, in Fig. 6(a) for $N_a = 9$, when $\tilde{\mu} = 10^5$, there is no noticeable compared to the results for the plate without any hinge. In contrast, in Fig. 6(b) for $N_a = 99$, subtle differences remain between the results for $\tilde{\mu} = 10^5$ and the single-plate case, and a much larger $\tilde{\mu}$ is required to achieve consistency.

In addition to the wave run-up on the beach, the deflection and principal strain in the elastic plates are also considered. From Eq. (24), we obtain

$$\eta^{(3)}(x) = \frac{ih_0}{\omega}\frac{d^2\phi^{(3)}}{dx^2} = \frac{ih_0}{\omega} \times \left\{ \begin{array}{c} -\sum_{m=-2}^{0} \kappa_m^2 \left(C_m e^{i\kappa_m x} + D_m e^{-i\kappa_m x}\right) \\ +\sum_{i=1}^{N_a} E_i \frac{\partial^4 G(x,a_i)}{\partial x^2 \partial \zeta^2} + \sum_{i=1}^{N_b} F_i \frac{\partial^2 G(x,b_i)}{\partial x^2} \end{array} \right\}. \quad (44)$$

The principal strain can be calculated from[31]

$$\varepsilon^{(3)}(x) = \frac{h_e}{2}\frac{d^2\eta^{(3)}(x)}{dx^2} = \frac{ih_0h_e}{2\omega} \times \left\{ \begin{array}{c} \sum_{m=-2}^{0} \kappa_m^4 \left(C_m e^{i\kappa_m x} + D_m e^{-i\kappa_m x}\right) \\ +\sum_{i=1}^{N_a} E_i \frac{\partial^6 G(x,a_i)}{\partial x^4 \partial \zeta^2} + \sum_{i=1}^{N_b} F_i \frac{\partial^4 G(x,b_i)}{\partial x^4} \end{array} \right\}. \quad (45)$$

At a given wave frequency, the maximum deflection and the maximum principal strain in the beam are represented by η_{max} and ε_{max} respectively. These values can be determined through a numerical search over a sufficient number of points along the beam.

For the 10-plate system ($N_a = 9$) mentioned for Fig. 6(a), the η_{max} and ε_{max} vs k_0h_0 are presented in Figs. 7(a) and 7(b). In Fig. 7(a), when k_0h_0 is small or the wavelength is very large, η_{max} for the four different values of $\tilde{\mu}$ are nearly identical. As k_0h_0 increases, irregular oscillations appear in the curves. When $\tilde{\mu} = 0$, the oscillation amplitude is very small. As $\tilde{\mu}$ increases, the oscillatory behaviour of η_{max} vs k_0h_0 gradually becomes more pronounced, and the results approach the single-elastic-plate case as $\tilde{\mu} \to +\infty$. By contrast, in Fig. 7(b), ε_{max} in the four cases generally increases with k_0h_0 and varies more smoothly, with much less pronounced fluctuations. Additionally, it is interesting to see that at $k_0h_0 = 0.0605$ and 0.1813, local minimums can be observed in η_{max} for all four cases.

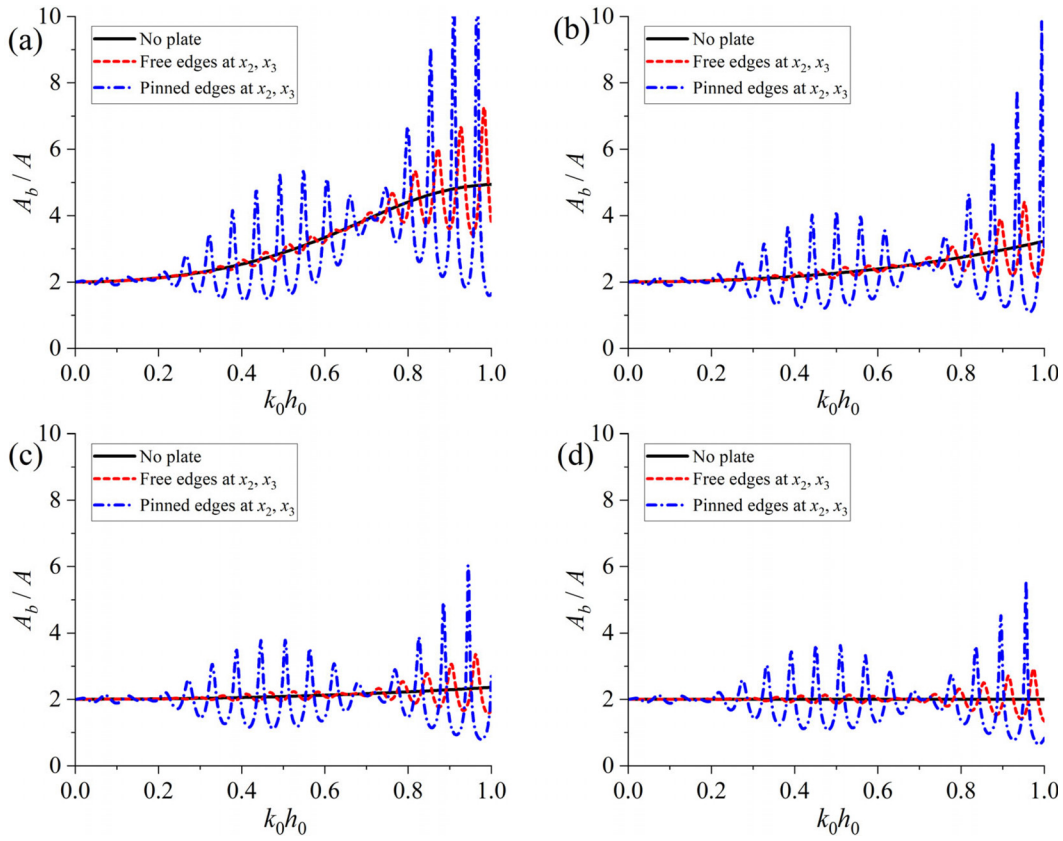

FIG. 5. Wave run-up on the beach vs k_0h_0 under different inclined angle β. (a) $\beta = 30^o$; (b) $\beta = 45^o$; (c) $\beta = 60^o$; and (d) $\beta = 90^o$. ($d/h_0 = 10$, $(x_2 - x_1)/h_0 = 50$, $N_a = N_b = 0$)

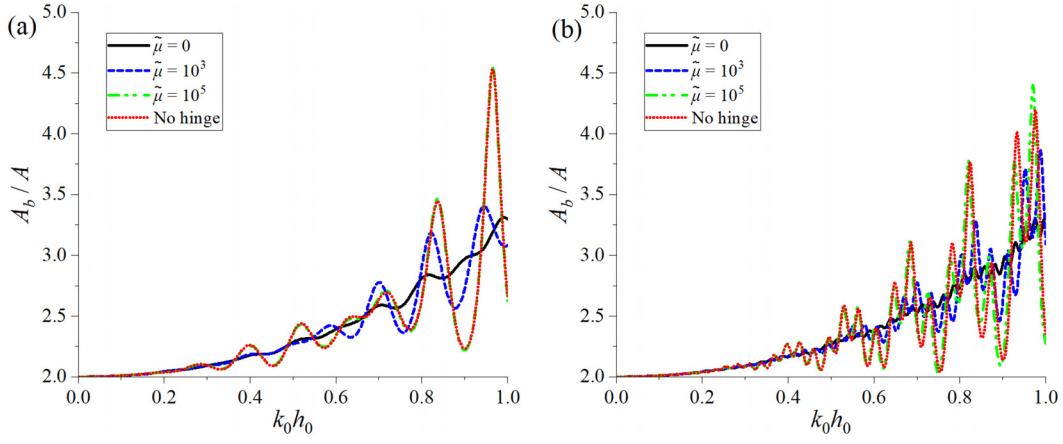

FIG. 6. Wave run-up on the beach vs k_0h_0 under different numbers of plates and various rotational spring stiffnesses. (a) $N_a = 9$; (b) $N_a = 99$. ($d/h_0 = 1$, $(x_2 - x_1)/h_0 = 20$, $\beta = 45^o$, $N_b = 0$, free edges at $x = x_2$ & x_3).

Particularly, at $k_0h_0 = 0.0605$, η_{max}/A is minimum and approximately to be 0.615. The corresponding plate deflection distributions are shown in Figs. 8(a) and 8(b). In general, the deflection distributions in all cases are quite similar and nearly symmetric about the center of the plate, with the maximum deflection occurring at the ends of the plate system. In contrast, significant differences are observed in the principal strain distribution across these cases, as shown in Fig. 9.

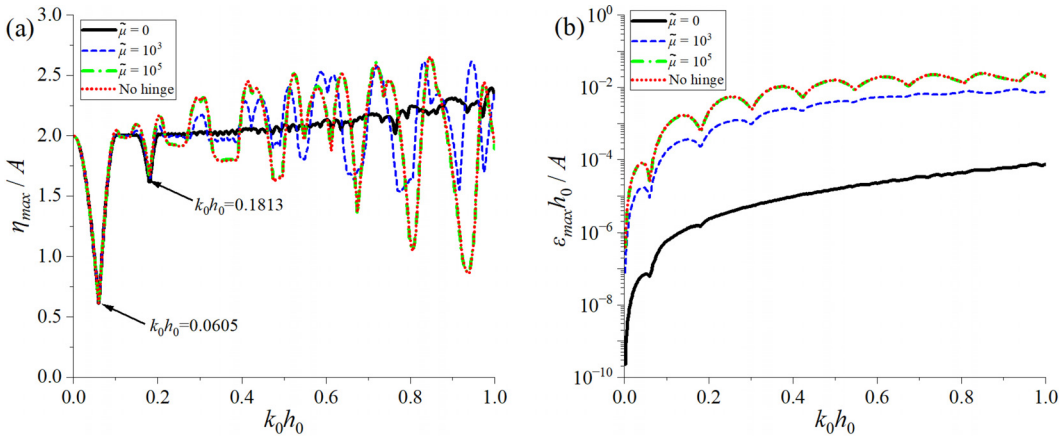

FIG. 7. The maximum deflection (a) and the maximum principal strain (b) vs k_0h_0 under various rotational spring stiffness. ($d/h_0 = 1$, $(x_2 - x_1)/h_0 = 20$, $\beta = 45^o$, $N_a = 9$, $N_b = 0$, free edges at $x = x_2$ & x_3)

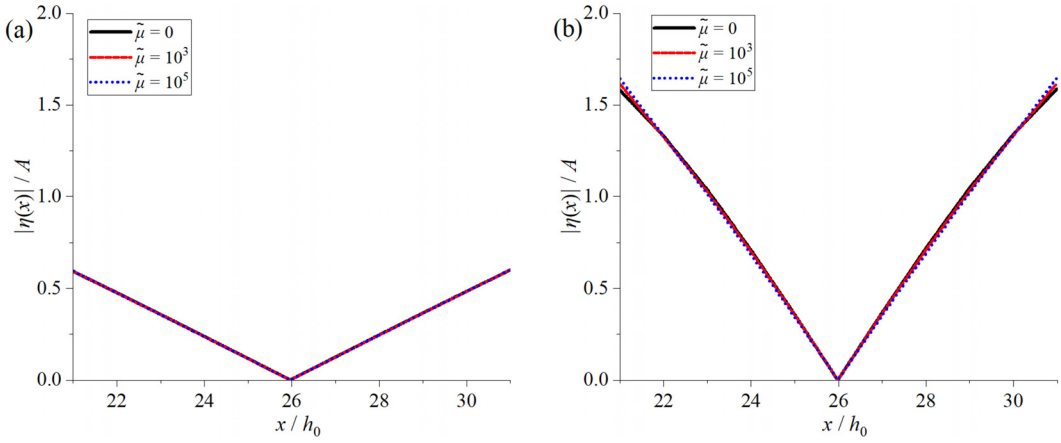

FIG. 8. Deflection distribution in the elastic plates. (a) $k_0h_0 = 0.0605$; (b) $k_0h_0 = 0.1813$. ($d/h_0 = 1$, $(x_2 - x_1)/h_0 = 20$, $\beta = 45^o$, $N_a = 9$, $N_b = 0$, free edges at $x = x_2$ & x_3)

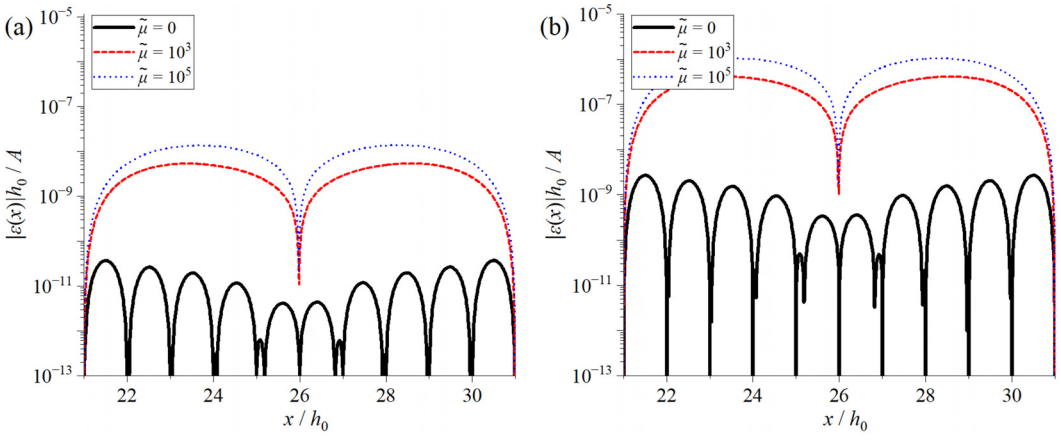

FIG. 9. Principal strain distribution in the elastic plates. (a) $k_0h_0 = 0.0605$; (b) $k_0h_0 = 0.1813$. ($d/h_0 = 1$, $(x_2 - x_1)/h_0 = 20$, $\beta = 45^o$, $N_a = 9$, $N_b = 0$, free edges at $x = x_2$ & x_3)

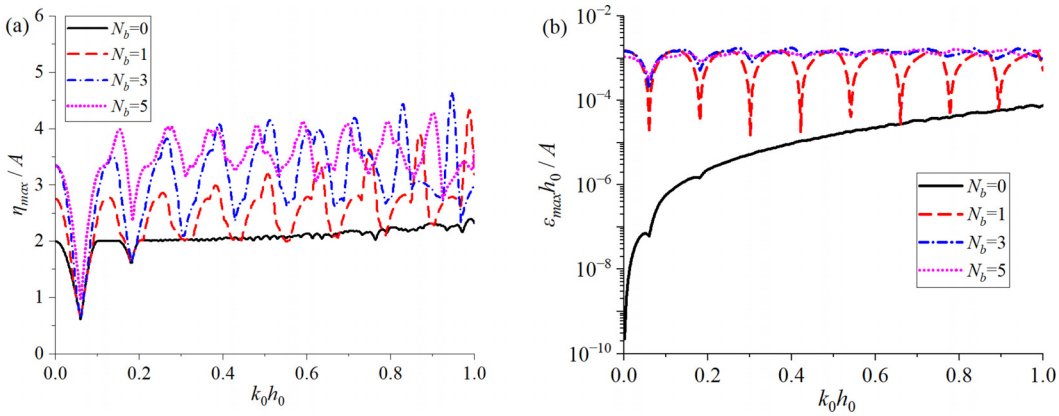

FIG. 10. The maximum deflection (a) and the maximum principal strain (b) vs k_0h_0 under different numbers of vertical spring supports. ($d/h_0 = 1$, $(x_2 - x_1)/h_0 = 20$, $\beta = 45°$, $N_a = 9$, free edges at $x = x_2$ & x_3, $\tilde{\mu} = 0$, $\tilde{q} = 20$)

We also consider scenarios in which multiple plate systems are both hinged by rotational springs and supported by vertical springs, or $N_b \neq 0$. In this case, we may assume that each vertical spring has the identical stiffness as $\tilde{q}^{(i)} = \tilde{q}$ $(i = 1 \sim N_b)$. We may consider three different vertical spring arrangements for the above 10 hinged plates system with $\tilde{\mu} = 0$ and $\tilde{q} = 20$. In particular, Case 1: $N_b = 1$, $b_1 = a_5$; Case 2: $N_b = 3$, $b_i = a_{2i+1}$ $(i = 1 \sim 3)$; Case 3: $N_b = 5$, $b_i = a_{2i-1}$ $(i = 1 \sim 5)$. The results of the maximum deflection and the maximum principal strain are shown in Fig. 10. In the considered range, for most values of k_0h_0, both the magnitude of η_{max} and ε_{max} increase due to the presence of the vertical springs. In Fig. 10(a), when N_b is nonzero, the fluctuation behaviour of η_{max} vs k_0h_0 becomes much more pronounced compared to the case with $N_b = 0$. In Fig. 10(b), when $N_b = 1$, ε_{max} oscillates with k_0h_0, which differs significantly from the variation trend observed for $N_b = 0$. As N_b increases further, the oscillations gradually diminish.

C. Time-domain analysis of wave interaction with floating elastic plates

Apart from the frequency domain results shown above, the time-domain analysis is also extended here. Based on the wave elevation $\eta(x, \omega)$ of the fluid surface by Eqs. (3) and (44), the time-domain wave elevation $\hat{\eta}(x, t)$ can be constructed from

$$\hat{\eta}(x,t) = \mathrm{Re}\left\{\frac{1}{\pi}\int_0^{+\infty} f(\omega)\eta(x,\omega)e^{\mathrm{i}\omega t}d\omega\right\}, \tag{46}$$

where $f(\omega)$ denotes the Fourier transform of an incident wave pulse. Here, we may first assume the incident wave pulse is a Gaussian wave packet, or $f(\omega) = \sqrt{\pi\gamma}e^{-\gamma(\omega-\omega_0)^2}$, where γ and ω_0 represent the spreading function and centre frequency respectively. Here, case studies are conducted with $\gamma = 20\,\mathrm{s}^2\,\mathrm{rad}^{-2}$ and $\omega_0 = 2\,\mathrm{rad\,s}^{-1}$. The time t is nondimensionalized by $\tau = t\sqrt{g/h_0}$.

The results of a single plate floating near a beach with the sloping angle $\beta = 10°$ are shown in Figs. 11 and 12, where Fig. 11 is for the plate with free edges at x_2 and x_3 and Fig. 12 is for pinned edges. From $\tau = -50$ to $\tau = 200$, the interaction between the incoming waves and the floating plate is clearly demonstrated, including the wave-induced deflection and the waves reflected by the beach. These reflected waves then further interact with the plates, showcasing the phenomenon of multiple wave scattering. Notably, the initial wave packet is split into several smaller packets as a result of its interaction with both the plate and the beach. Over a long period of time, the disturbed fluid surface gradually stabilizes. Furthermore, the comparison between Figs. 11 and 12 highlights the impact of plate edge constraints on wave transmission and reflection. A similar analysis is also made in the case of three elastic plates connected by rotational hinges, as shown in Fig. 13.

In addition to incident waves of Gaussian wave packets, a storm wave-type incident pulse is also considered. To achieve this, we may introduce a Gaussian-type wave profile with amplitude A, or

$$\xi_0(x) = Ae^{-\nu(x-x_p)^2}, \tag{47}$$

where x_p denotes the peak position of the wave, ν is a typical parameter control the shape of the wave profile, and $\nu = 0.001\,\mathrm{m}^{-2}$ is selected here. In Eq. (47), x_p should be selected to be far from the floating plates and the beach, or $\xi_0 \to 0$ near these positions, here, we may use $x_p = 50h_0$ here. Based on Meylan[32] and Hazard and Meylan,[33] the time-domain wave elevation can be constructed from

$$\hat{\eta}(x,t) = \mathrm{Re}\left\{\frac{1}{\pi}\int_0^{+\infty}\left[P(k)\eta(x,\omega) - \tilde{\xi}_0(k)e^{-\mathrm{i}kx}\right]e^{\mathrm{i}\omega t}dk\right\}, \tag{48}$$

where $\omega = k\sqrt{gh}$, and

$$P(k) = \int_0^{+\infty}\xi_0(x)\bar{\eta}(x,\omega)dx \tag{49a}$$

$$\tilde{\xi}_0(k) = \int_0^{+\infty}\xi_0(x)e^{\mathrm{i}kx}dx, \tag{49b}$$

with $\bar{\eta}$ denotes the conjugate of η. Compared with the transform formula in Eq. (46), some modifications are in fact imposed to Eq. (48) to account for the single direction of incident propagation. Particularly, the second term in Eq. (48) is introduced to cancel the pulse travelling away to $x = +\infty$. Based on the established time-domain models, case

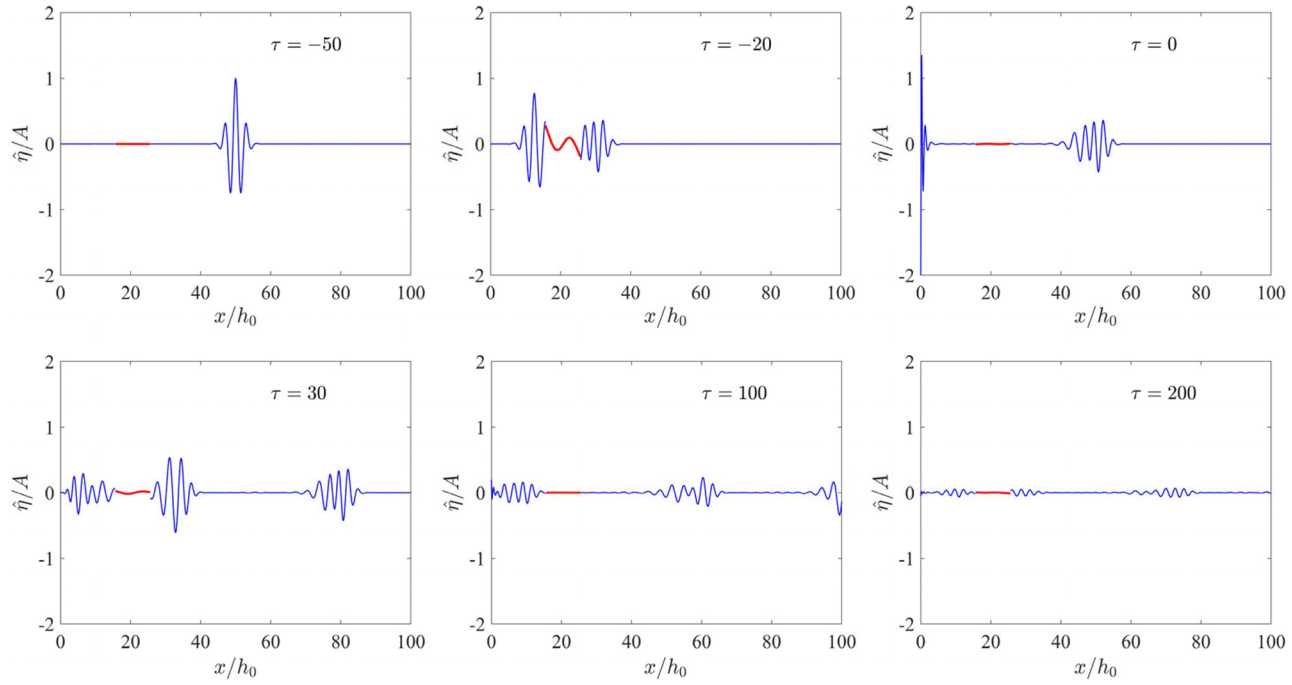

FIG. 11. Wave profiles at six different time steps for the case of a Gaussian wave packet incident pulse interaction with a single floating plate ($\beta = 10^o$, $d/h_0 = 10$, $(x_2 - x_1)/h_0 = 10$, free edges at $x = x_2$ & x_3; Red line: plate deflection; Blue line: surface wave profile). Multimedia available online.

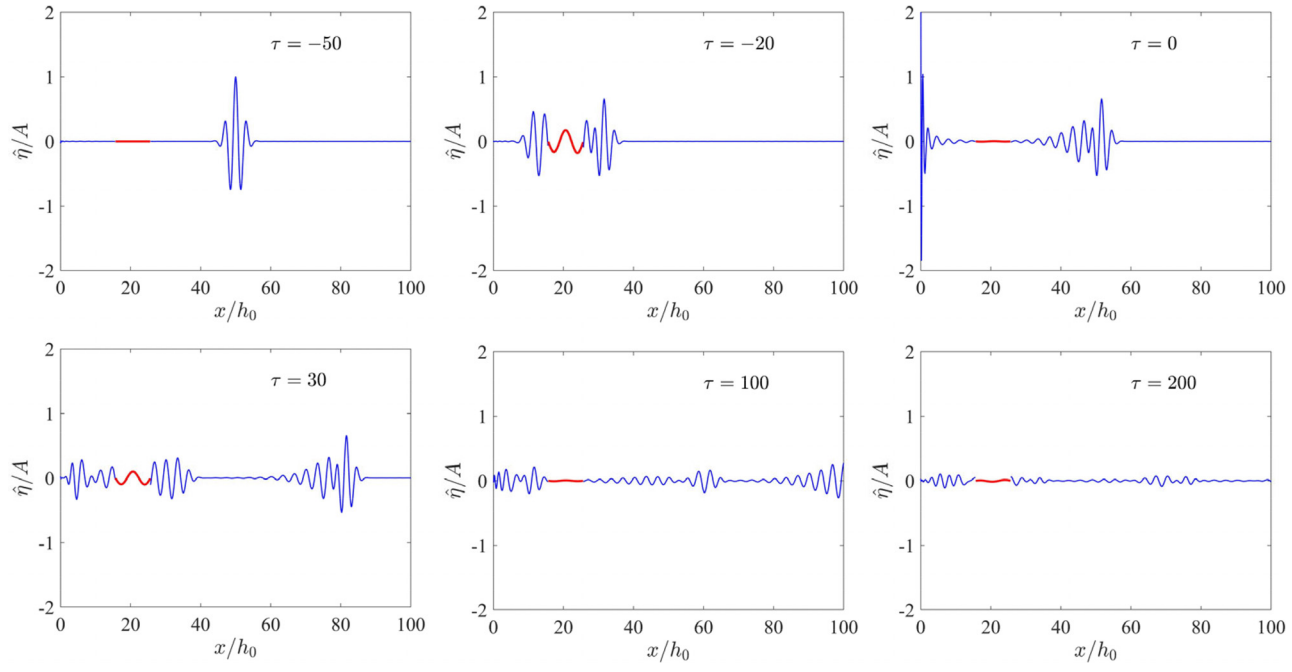

FIG. 12. Wave profiles at six different time steps for the case of a Gaussian wave packet incident pulse interaction with a single floating plate ($\beta = 10^o$, $d/h_0 = 10$, $(x_2 - x_1)/h_0 = 10$, pinned edges at $x = x_2$ & x_3; Red line: plate deflection; Blue line: surface wave profile). Multimedia available online.

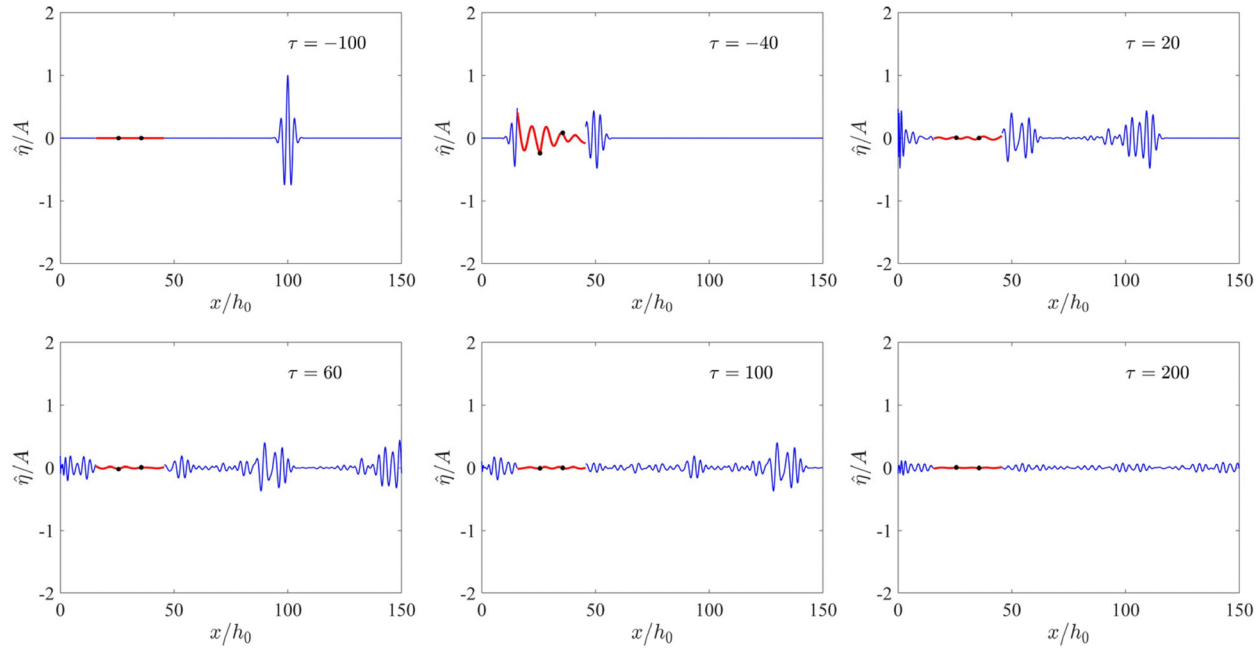

FIG. 13. Wave profiles at six different time steps for the case of a Gaussian wave packet incident pulse interaction with three floating plates ($\beta = 10^o$, $d/h_0 = 10$, $(x_2 - x_1)/h_0 = 10$, free edges at $x = x_2$ & x_3, $N_a = 2$, $N_b = 0$, $\tilde{\mu} = 10^3$; Red line: plate deflection; Blue line: surface wave profile; Black dot: rotational hinges). Multimedia available online.

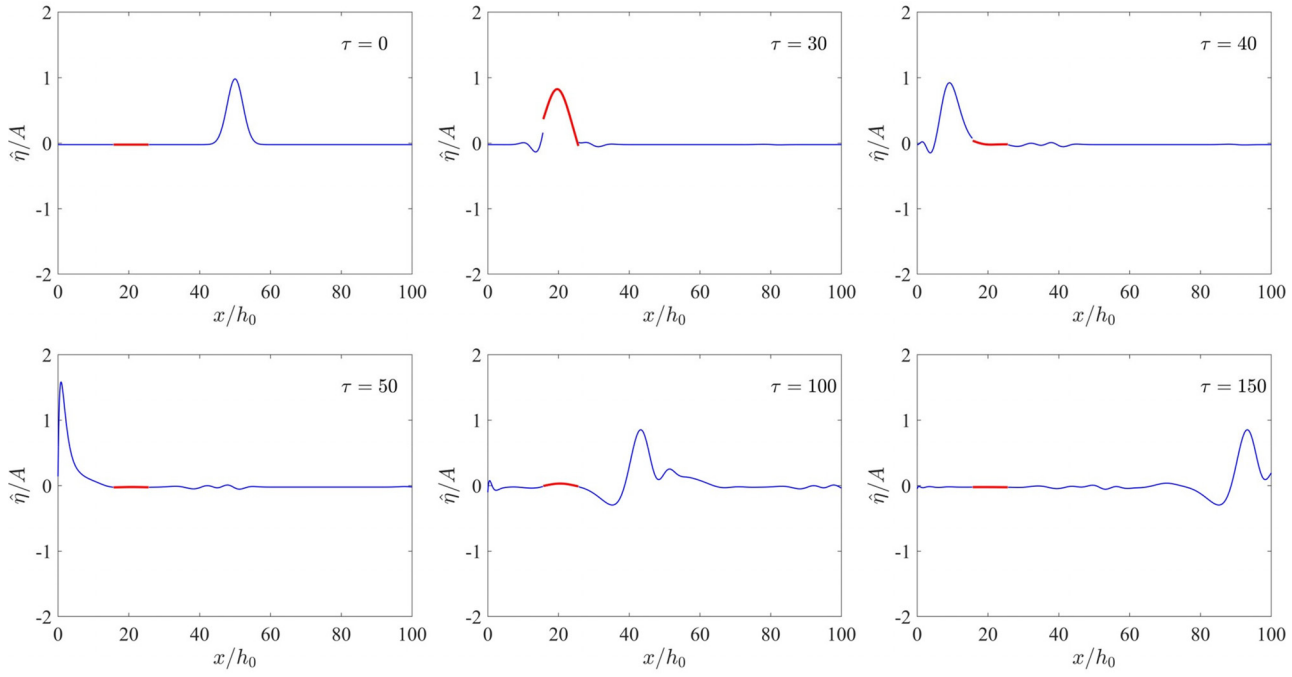

FIG. 14. Wave profiles at six different time steps for the case of a storm wave-type incident pulse interaction with a single floating plate ($\beta = 10^o$, $d/h_0 = 10$, $(x_2 - x_1)/h_0 = 10$, free edges at $x = x_2$ & x_3; Red line: plate deflection; Blue line: surface wave profile). Multimedia available online.

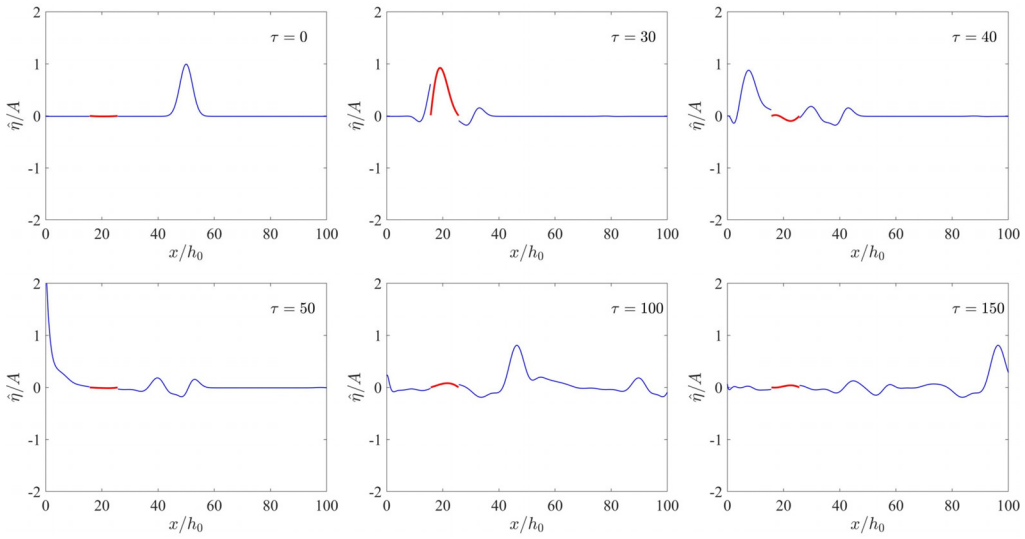

FIG. 15. Wave profiles at six different time steps for the case of a storm wave-type incident pulse interaction with a single floating plate ($\beta = 10^o$, $d/h_0 = 10$, $(x_2 - x_1)/h_0 = 10$, pinned edges at $x = x_2$ & x_3; Red line: plate deflection; Blue line: surface wave profile). Multimedia available online.

studies are conducted for a single plate floating near a beach with $\beta = 10^o$, as shown in Figs. 14 and 15 for the plate with free and pinned edges at $x = x_2$ & x_3 respectively.

V. CONCLUSIONS

The interaction of waves with single and multiple elastic plates floating near a sloping beach is studied analytically. The solution approach is based on linearized velocity potential theory with the shallow water assumption for the fluid, along with Kirchhoff–Love plate theory for the elastic plates. In this approach, the velocity potentials in the free surface regions with flat seabed are expanded into a series of eigenfunctions with unknown coefficients, while the velocity potential of the fluid beneath the plates is constructed using the Green function method. In the sloping beach region, a variable substitution procedure is applied to the BVP to obtain the general solution. The velocity potential and horizontal velocity are then matched at the interface of each fluid domain to derive the final solution. This treatment significantly reduces the number of unknowns, when compared to the procedure that only involves the MEE. Besides, the established procedure is applicable to arbitrary types of physical constraints in the elastic plate system.

Case studies are first conducted for a single floating elastic plate. As the length of the plate tends to be 0, the wave run-up on the beach is found to be consistent with the case without any plate in the literature, which verifies the present model. Besides, with the presence of the plate, it is found that the wave run-up fluctuates with the wave number k_0h_0. These fluctuations are primarily caused by two factors. On the one hand, the transmission and reflection of waves by the floating plates induce oscillations in the wave run-up, with the oscillation becoming evident as the plate length increases. Second, the fluctuation is also influenced by wave propagation between the beach and the plate, particularly when there is a large gap between the plate and the beach. In such a case, a wide space-approximated solution is further proposed to explain such an oscillatory phenomenon.

In addition to the case of a single plate, computations are also performed for multiple plates connected by rotational springs. The numerical results indicate that the maximum plate deflection oscillates with k_0h_0, while the maximum principal strain varies more smoothly. Furthermore, the stiffness of the rotational springs can significantly impact both the maximum deflection and principal strain. An analysis is also conducted on a plate system consisting of both rotational springs and vertical springs, which helps capture the structural response characteristics of such plates system.

In this paper, in addition to the frequency-domain investigations, time-domain analyses are also considered. Case studies are also conducted based on two types of incident impulses. Particularly, the Gaussian wave packets and a storm-wave type. The numerical results illustrate the dynamic interaction between waves and floating elastic plates, as well as the reflection of waves by the sloping wall. Additionally, the results reveal the phenomenon of multiple wave scattering.

The work primarily provides theoretical insights into the hydrodynamic responses of FSFs deployed near coastal regions, contributing to a better understanding of wave-induced deflection and strain in floating structures, which is valuable for their design and optimisation. Additionally, the results of wave run-up on the beach offer insights into how the deployment of FSFs influences wave behaviour in coastal regions.

SUPPLEMENTARY MATERIAL

See the supplementary material for the MATLAB codes to analyse the interaction between irregular waves and floating elastic plates in time-domain is supplied, which corresponds to the results shown in Figs. 11–15 in Sec. IV C.

ACKNOWLEDGMENTS

L.H. acknowledges grants received from Innovate UK (Nos. 10048187, 10079774, and 10081314), the Royal Society (IEC\NSFC

\223253, RG R2 232462), and UK Department for Transport (TRIG2023—No. 30066).

AUTHOR DECLARATIONS

Conflict of Interest

The authors have no conflicts to disclose.

Author Contributions

Yifeng Yang: Investigation (lead); Methodology (equal); Software (equal); Validation (lead); Writing – original draft (lead). **Luofeng Huang:** Conceptualization (lead); Funding acquisition (lead); Project administration (equal); Writing – original draft (equal); Writing – review & editing (equal). **Michael Howard Meylan:** Methodology (equal); Project administration (equal); Software (equal); Supervision (lead); Writing – original draft (equal); Writing – review & editing (equal).

DATA AVAILABILITY

The data that support the findings of this study are available from the corresponding authors upon reasonable request.

REFERENCES

[1]A. Sahu, N. Yadav, and K. Sudhakar, "Floating photovoltaic power plant: A review," Renewable Sustainable Energy Rev. **66**, 815 (2016).
[2]S. Benjamins, B. Williamson, S.-L. Billing, Z. Yuan, M. Collu, C. Fox, L. Hobbs, E. A. Masden, E. J. Cottier-Cook, and B. Wilson, "Potential environmental impacts of floating solar photovoltaic systems," Renewable Sustainable Energy Rev. **199**, 114463 (2024).
[3]C. Fox and V. A. Squire, "Reflection and transmission characteristics at the edge of shore fast sea ice," J. Geophys. Res.: Oceans **95**, 11629, https://doi.org/10.1029/JC095iC07p11629 (1990).
[4]L. A. Tkacheva, "Scattering of surface waves by the edge of a floating elastic plate," J. Appl. Mech. Tech. Phys. **42**, 638 (2001).
[5]M. H. Meylan and V. A. Squire, "The response of ice floes to ocean waves," J. Geophys. Res.: Oceans **99**, 891, https://doi.org/10.1029/93JC02695 (1994).
[6]D. V. Evans and R. Porter, "Wave scattering by narrow cracks in ice sheets floating on water of finite depth," J. Fluid Mech. **484**, 143 (2003).
[7]R. Porter and D. V. Evans, "Scattering of flexural waves by multiple narrow cracks in ice sheets floating on water," Wave Motion **43**, 425 (2006).
[8]T. D. Williams and V. A. Squire, "Scattering of flexural–gravity waves at the boundaries between three floating sheets with applications," J. Fluid Mech. **569**, 113 (2006).
[9]S. C. Barman, S. Das, T. Sahoo, and M. H. Meylan, "Scattering of flexural-gravity waves by a crack in a floating ice sheet due to mode conversion during blocking," J. Fluid Mech. **916**, A11 (2021).
[10]V. A. Squire, "Of ocean waves and sea-ice revisited," Cold Reg. Sci. Technol. **49**, 110 (2007).
[11]D. Karmakar, J. Bhattacharjee, and T. Sahoo, "Wave interaction with multiple articulated floating elastic plates," J. Fluids Struct. **25**, 1065 (2009).
[12]D. Karmakar and C. G. Soares, "Scattering of gravity waves by a moored finite floating elastic plate," Appl. Ocean Res. **34**, 135 (2012).
[13]S. Singla, T. Sahoo, S. Martha, and H. Behera, "Effect of a floating permeable plate on the hydroelastic response of a very large floating structure," J. Eng. Math. **116**, 49 (2019).
[14]K. M. Praveen, D. Karmakar, and C. Guedes Soares, "Hydroelastic analysis of periodic arrays of multiple articulated floating elastic plate," Ships Offshore Struct. **15**, 280 (2020).
[15]Y. F. Yang, K. Ren, B. Z. Zhou, S. Y. Sun, and L. F. Huang, "Wave interaction with multiple adjacent floating solar panels with arbitrary constraints," Phys. Fluids **36**, 037121 (2024).
[16]C. D. Wang and M. H. Meylan, "The linear wave response of a floating thin plate on water of variable depth," Appl. Ocean Res. **24**, 163 (2002).
[17]K. Belibassakis and G. Athanassoulis, "A coupled-mode model for the hydroelastic analysis of large floating bodies over variable bathymetry regions," J. Fluid Mech. **531**, 221 (2005).
[18]K. Belibassakis and G. Athanassoulis, "A coupled-mode technique for weakly nonlinear wave interaction with large floating structures lying over variable bathymetry regions," Appl. Ocean Res. **28**, 59 (2006).
[19]K. Belibassakis, "A boundary element method for the hydrodynamic analysis of floating bodies in variable bathymetry regions," Eng. Anal. Bound. Elem. **32**, 796 (2008).
[20]R. Porter and J. Newman, "Cloaking of a vertical cylinder in waves using variable bathymetry," J. Fluid Mech. **750**, 124 (2014).
[21]A. Feng, W. Bai, and W. Price, "Two-dimensional wave radiation and diffraction problems in a flat or sloping seabed environment," J. Fluids Struct. **75**, 193 (2017).
[22]X. Liu, X. Wang, and S. Xu, "A DMM-EMM-RSM hybrid technique on two-dimensional frequency-domain hydroelasticity of floating structures over variable bathymetry," Ocean Eng. **201**, 107135 (2020).
[23]P. Kar, T. Sahoo, and M. Meylan, "Bragg scattering of long waves by an array of floating flexible plates in the presence of multiple submerged trenches," Phys. Fluids **32**, 096603 (2020).
[24]C. W. Zhang, P. F. Wang, L. F. Huang, M. K. Zhang, H. T. Wu, and D. Z. Ning, "Resonance mechanism of hydroelastic response of multi-patch floating photovoltaic structure in water waves over stepped seabed," Phys. Fluids **35**, 107137 (2023).
[25]G. B. Whitham, *Linear and Nonlinear Waves* (Wiley, 2011).
[26]R. G. Dean and R. A. Dalrymple, *Water Wave Mechanics for Engineers and Scientists* (World Scientific Publishing Company, 1991).
[27]D. W. Xia, J. W. Kim, and R. C. Ertekin, "On the hydroelastic behavior of two-dimensional articulated plates," Mar. Struct. **13**, 261 (2000).
[28]C. E. Synolakis, "The runup of solitary waves," J. Fluid Mech. **185**, 523 (1987).
[29]J. B. Keller and H. B. Keller, *Water Wave Run-Up on a Beach* (Office of Naval Research, 1964).
[30]M. Meylan and V. A. Squire, "Finite-floe wave reflection and transmission coefficients from a semi-infinite model," J. Geophys. Res.: Oceans **98**, 12537, https://doi.org/10.1029/93JC00940 (1993).
[31]S. P. Timoshenko and S. Woinowsky-Krieger, *Theory of Plates and Shells* (McGraw-Hill, 1959).
[32]M. H. Meylan, "Spectral solution of time-dependent shallow water hydroelasticity," J. Fluid Mech. **454**, 387 (2002).
[33]C. Hazard and M. H. Meylan, "Spectral theory for an elastic thin plate floating on water of finite depth," SIAM J. Appl. Math. **68**, 629 (2008).